JACS
JOURNAL OF THE AMERICAN CHEMICAL SOCIETY

ARTICLE

pubs.acs.org/JACS

Explorations of New Second-Order Nonlinear Optical Materials in the Potassium Vanadyl Iodate System

Chuan-Fu Sun,[†,‡] Chun-Li Hu,[†] Xiang Xu,[†] Bing-Ping Yang,[†] and Jiang-Gao Mao*[,†]

[†]State Key Laboratory of Structural Chemistry, Fujian Institute of Research on the Structure of Matter, Chinese Academy of Sciences, Fuzhou 350002, People's Republic of China

[‡]Graduate School of the Chinese Academy of Sciences, Beijing 100039, People's Republic of China

Supporting Information

ABSTRACT: Four new potassium vanadyl iodates based on lone-pair-containing IO_3 and second-order Jahn−Teller distorted VO_5 or VO_6 asymmetric units, namely, α-$KVO_2(IO_3)_2(H_2O)$ (*Pbca*), β-$KVO_2(IO_3)_2(H_2O)$ ($P2_12_12_1$), $K_4[(VO)(IO_3)_5]_2(HIO_3)(H_2O)_2\cdot H_2O$ (*P*1), and $K(VO)_2O_2(IO_3)_3$ (*Ima*2) have been successfully synthesized by hydrothermal reactions. α-$KVO_2(IO_3)_2(H_2O)$ and β-$KVO_2(IO_3)_2(H_2O)$ exhibit two different types of 1D $[VO_2(IO_3)_2]^-$ anionic chains. Neighboring VO_6 octahedra in the α-phase are corner-sharing into a 1D chain with the IO_3 groups attached on both sides of the chain in a uni- or bidentate bridging fashion, whereas those of VO_5 polyhedra in the β-phase are bridged by IO_3 groups into a right-handed helical chain with remaining IO_3 groups being grafted unidentately on both sides of the helical chain. The structure of $K_4[(VO)(IO_3)_5]_2(HIO_3)(H_2O)_2\cdot H_2O$ contains novel isolated $[(VO)(IO_3)_5]^{2-}$ units composed of one VO_6 octahedron linked to five IO_3 groups and one terminal O^{2-} anion. The structure of $K(VO)_2O_2(IO_3)_3$ exhibits a 1D $[(VO)_2O_2(IO_3)_3]^-$ chain in which neighboring VO_6 octahedra are interconnected by both oxo and bridging iodate anions. Most interestingly, three of four compounds are noncentrosymmetric (NCS), and $K(VO)_2O_2(IO_3)_3$ displays a very strong second-harmonic generation response of about 3.6 × KTP, which is phase matchable. It also has high thermal stability, a wide transparent region and moderate hardness as well as an excellent growth habit. Thermal analyses and optical and ferroelectric properties as well as theoretical calculations have also been performed.

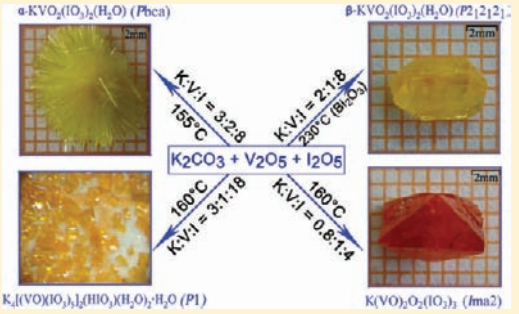

INTRODUCTION

The search for new second-order nonlinear optical (NLO) materials is of current interest and great importance due to their applications in photonic technologies, such as laser frequency conversion, optical parameter oscillator (OPO), and signal communication.[1] In the past decades, significant efforts have been made for the discoveries of new NLO crystals, which have brought considerably useful NLO materials, such as β-BaB_2O_4 (BBO), LiB_3O_5 (LBO), KH_2PO_4 (KDP), $KTiOPO_4$ (KTP), $LiNbO_3$ (LN), $ZnGeP_2$, and $AgGaSe_2$.[2,3] For an ideal second-harmonic generation (SHG) material, it should possesses high SHG coefficient, wide transparent region, a moderate laser damage threshold, high thermal stability, phase matchability, and easy to grow large-size crystals. However, many of the NLO materials used currently still have shortcomings of one kind or another which has limited their applications. For example, KDP shows a low SHG effect and is moisture sensitive, whereas $AgGaSe_2$ has a low laser damage threshold and is difficult to grow high-quality large-single crystals. Therefore, the searching for better NLO materials is still a hot research topic and a difficult challenge.

The prerequisite for a SHG material is that it should have a noncentrosymmetric (NCS) structure. It is found that a compound with asymmetric building units is more likely to form NCS structure. As for the metal-oxide-based system, there are mainly three types of inorganic asymmetric units which favor NLO activity, including planar $(BO_3)^{3-}$ with a π-conjugated system,[4] second-order Jahn−Teller (SOJT) distorted d^0 early transition-metal cations (e.g., Nb^{5+}, V^{5+}, Mo^{6+}),[5] and stereochemically active lone pairs (e.g., SeO_3^{2-}, IO_3^-, Pb^{2+}, Bi^{3+}).[6] It has been demonstrated that the combination of multiple types of asymmetric units in the same compound is an effective synthetic route for new inorganic solids with excellent SHG properties if those units are properly aligned.[7,8]

Recently, metal iodates such as α-$LiIO_3$ and $Cs_2I_4O_{11}$ have become an important class of NLO materials due to their excellent overall properties.[6a,b,9] Furthermore, d^0 early transition-metal cations (e.g., Nb^{5+}, V^{5+}, Mo^{6+}) have been introduced into the metal iodates to enhance their SHG responses by means of the additive polarizations of both types of asymmetric units,[10−12] e.g., $BaNbO(IO_3)_5$ displays a very large SHG response of 14 × KDP.[12a] Such types of NLO materials are dominantly alkali and alkaline earth compounds. Studies also

Received: January 11, 2011
Published: March 23, 2011

ACS Publications © 2011 American Chemical Society

dx.doi.org/10.1021/ja200257a | *J. Am. Chem. Soc.* 2011, 133, 5561–5572

have revealed that the size of alkali or alkaline earth metal ion has a great influence on the compositions, structures, and SHG properties of the materials formed. For example, $Li_2Ti(IO_3)_6$ and $Na_2Ti(IO_3)_6$ are isostructural and polar with strong SHG responses of 500 and 400 times that of α-SiO_2, respectively, whereas $M_2Ti(IO_3)_6$ (M = K, Rb, Cs, Tl) is structurally centrosymmetric (CS). So far, little is known about the effect of the reaction conditions (such as reaction ratio, temperature, and pH value) on the structures and the properties of materials isolated within a same reaction system. We deem that such studies are also very interesting and important for understanding the structure−property relationships as well as the exploration of new NLO materials. In this paper, we focused on the potassium vanadyl iodate system. Though a number of metal vanadyl iodates have been reported,[10b,12b,13] only a few are noncentrosymmetric (NCS) and NLO-active, including isostructural $M[(VO)_2(IO_3)_3O_2]$ ($M = Rb^+, Cs^+, NH_4^+$) with a SHG response of 500 × α-SiO_2 for the cesium phase,[10b] $NaVO_2(IO_3)_2(H_2O)$ with a large SHG response of 20 × KDP (KH_2PO_4) or 800 × α-SiO_2,[12b] and $LaVO_2(IO_3)_4\cdot H_2O$ with a weak SHG response of 0.2 × KDP.[13e] Our systematic explorations of new NLO materials in the unexplored K−V−I−O quaternary system resulted in four new potassium vanadyl iodates, namely, α-$KVO_2(IO_3)_2(H_2O)$, β-$KVO_2(IO_3)_2(H_2O)$, $K_4[(VO)(IO_3)_5]_2(HIO_3)(H_2O)_2\cdot H_2O$, and $K(VO)_2O_2(IO_3)_3$. They exhibit three different 1D anionic chains and a 0D anionic cluster. More importantly, three of the four compounds are NCS, among which $K(VO)_2O_2(IO_3)_3$ displays a very strong SHG efficiency of about 3.6 times that of KTP ($KTiOPO_4$). Herein, we report their syntheses, crystal structures, and electronic and NLO properties.

EXPERIMENTAL SECTION

Materials and Instruments. All of the chemicals were analytically pure from commercial sources and used without further purification. K_2CO_3, V_2O_5, and I_2O_5 were purchased from the Shanghai Reagent Factory (AR, 99.0+%).

IR spectra were recorded on a Magna 750 FT-IR spectrometer as KBr pellets in the range of 4000−400 cm^{-1}.

Microprobe elemental analyses were performed on a field emission scanning electron microscope (FESEM, JSM6700F) equipped with an energy dispersive X-ray spectroscope (EDS, Oxford INCA).

Powder X-ray diffraction patterns were collected on a Rigaku Miniflex Π powder diffractometer, using monochromated Cu−Kα radiation with a step size of 0.02°.

Thermogravimetric analyses and differential thermal analysis were carried out with NETZSCH STA 449C and NETZSCH DTA 404PC, respectively, at a heating rate of 10 °C/min under a N_2 atmosphere.

The UV−vis absorption and optical diffuse reflectance spectra were measured at room temperature with a PE λ 900 UV−vis spectrophotometer. $BaSO_4$ plate was used as a standard (100% reflectance). The absorption spectrum was calculated from reflectance spectra using the Kubelka−Munk function: $\alpha/S = (1 - R)^2/2R$,[14] where α is the absorption coefficient, S is the scattering coefficient, which is practically wavelength independent when the particle size is larger than 5 μm, and R is the reflectance.

The Vickers hardness measurements were carried out with the crystals on a 401 MVA Vickers hardness tester.

The measurements of SHG were carried out on the sieved powder samples by using the Kurtz and Perry method with a 2.05 μm Q-switch laser.[15] The SHG efficiency has been shown to depend strongly on particle size, thus the sample of $K(VO_2)_2(IO_3)_3$ was ground and sieved into several distinct particle size ranges (44−53, 53−74, 74−105, 105−149, 149−210, 210−270, and 270−325 μm). The sieved KTP powders were used as reference materials to assume the effect. All of the samples were placed in separate capillary tubes. No index-matching fluid was used in any of the experiments.

The ferroelectric properties of $K_4[(VO)(IO_3)_5]_2(HIO_3)(H_2O)_2\cdot H_2O$ and $K(VO)_2O_2(IO_3)_3$ were measured on an aixACCT TF Analyzer 2000 ferroelectric tester at room temperature. $K_4[(VO)(IO_3)_5]_2(HIO_3)(H_2O)_2\cdot H_2O$ powder was pressed into a pellet (5 mm diameter and 0.8 mm thick), and the conducting Ag glue was applied on the both sides of the pellet surfaces for electrodes. For $K(VO)_2O_2(IO_3)_3$, a single crystal was carefully burnished into a plate with a size of 5.8 × 1.86 × 1.46 mm^3 along [001] orientation, and the conducting Ag glue was applied on the both sides of the plate surfaces for electrodes.

Synthesis of α-$KVO_2(IO_3)_2(H_2O)$. A mixture of K_2CO_3 (0.1037 g, 0.75 mmol), V_2O_5 (0.0918 g, 0.50 mmol), I_2O_5 (0.6676 g, 2.00 mmol), and H_2O (2.0 mL) was sealed in an autoclave equipped with a Teflon liner (20 mL) and heated at 155 °C for 4 days, followed by slow cooling to room temperature at a rate of 3 °C/h. The final pH value is about 0.6. The reaction product was washed with water and ethanol and then dried in air. Yellow needle-shaped α-$KVO_2(IO_3)_2(H_2O)$ crystals were obtained as a single phase in a yield of about 95% based on V. Its purity was confirmed by XRD studies (Figure S1, Supporting Information). The energy-dispersive spectrometry (EDS) elemental analyses on several single crystals of α-$KVO_2(IO_3)_2(H_2O)$ gave an average molar ratio of K/V/I of 1.0: 1.0: 1.9, which is in good agreement with the one determined from single crystal X-ray structural analyses. IR data (KBr cm^{-1}): 3535 (m), 3426 (m), 1617 (m), 908 (m), 890 (m), 821 (m), 792 (s), 779 (s), 524 (w), 444 (m), 421 (w).

Synthesis of β-$KVO_2(IO_3)_2(H_2O)$. A mixture of K_2CO_3 (0.0692 g, 0.50 mmol), V_2O_5 (0.0455 g, 0.25 mmol), I_2O_5 (0.6676 g, 2.00 mmol), Bi_2O_3 (0.0047 g, 0.01 mmol), and H_2O (3.0 mL) was sealed in an autoclave equipped with a Teflon linear (20 mL) and heated at 230 °C for 4 days, followed by slow cooling to room temperature at a rate of 3 °C/h. The final pH value is about 0.6. The product was washed with water and ethanol and then dried in air. Large yellow plate-shaped β-$KVO_2(IO_3)_2(H_2O)$ crystals were obtained along with a small amount of colorless crystalline $Bi(IO_3)_3$ powders as impurity. After screening with a sieve (70 mesh), β-$KVO_2(IO_3)_2(H_2O)$ crystals were collected as a single phase in a yield of about 92% based on V. Its purity was confirmed by powder XRD studies (Figure S1, Supporting Information). The size of the single crystal has reached a maximum of 6 × 4 × 2 mm^3. When the reactions were carried out in absence of Bi_2O_3, only unknown amorphous phase could be isolated. Even a very small amount of Bi_2O_3 is enough for the formation of β-$KVO_2(IO_3)_2(H_2O)$. It is still not clear what kind of role Bi_2O_3 or the resultant $Bi(IO_3)_3$ played in the formation of β-$KVO_2(IO_3)_2(H_2O)$. The EDS elemental analyses on several single crystals of β-$KVO_2(IO_3)_2(H_2O)$ gave an average molar ratio of K/V/I of 1.0: 1.1: 2.1, which is in good agreement with the one determined from single crystal X-ray structural analyses. IR data (KBr cm^{-1}): 3137 (m), 1623 (m), 940 (m), 915 (s), 827 (m), 811 (m), 780 (s), 748 (m), 684 (s), 495 (m), 460 (m).

Synthesis of $K_4[(VO)(IO_3)_5]_2(HIO_3)(H_2O)_2\cdot H_2O$. A mixture of K_2CO_3 (0.2075 g, 1.50 mmol), V_2O_5 (0.0916 g, 0.50 mmol), I_2O_5 (3.0468 g, 9.00 mmol), and H_2O (5.0 mL) was sealed in an autoclave equipped with a Teflon linear (20 mL) and heated at 160 °C for 4 days, followed by slow cooling to room temperature at a rate of 3 °C/h. The final pH value is about 0.4. The product was washed with water and ethanol and then dried in air. Orange brick-shaped $K_4[(VO)(IO_3)_5]_2(HIO_3)(H_2O)_2\cdot H_2O$ crystals were obtained as a single phase in a yield of about 70% based on V. Its purity was confirmed by XRD studies (Figure S1, Supporting Information). The EDS elemental analyses on several single crystals of $K_4[(VO)(IO_3)_5]_2(HIO_3)(H_2O)_2\cdot H_2O$ gave an average molar ratio of K/V/I of 2.0: 1.1: 5.6, which is in good

dx.doi.org/10.1021/ja200257a | J. Am. Chem. Soc. 2011, 133, 5561–5572

Table 1. Crystal Data and Structural Refinements for the Four Compounds

formula	α-$KVO_2(IO_3)_2(H_2O)$	β-$KVO_2(IO_3)_2(H_2O)$	$K_4[(VO)(IO_3)_5]_2(HIO_3)(H_2O)_2\cdot H_2O$	$K(VO)_2O_2(IO_3)_3$
fw	489.86	489.86	2269.24	729.68
crystal system	orthorhombic	orthorhombic	triclinic	orthorhombic
space group	*Pbca* (no. 61)	$P2_12_12_1$ (no. 19)	*P*1 (no. 1)	*Ima*2 (no. 46)
a/Å	8.4998(6)	5.8083(14)	7.430(2)	14.136(3)
b/Å	7.2826(5)	8.793(2)	7.801(3)	10.2010(17)
c/Å	27.425(3)	16.785(4)	16.053(6)	8.0638(11)
α/°	90	90	97.207(3)	90
β/°	90	90	99.730(6)	90
γ/°	90	90	91.882(5)	90
V/Å^3	1697.6(2)	857.3(4)	908.4(5)	1162.8(3)
Z	8	4	1	4
D_{calcd}/g·cm^{-3}	3.833	3.795	4.148	4.168
μ(Mo−Kα)/mm^{-1}	8.955	8.867	10.443	9.997
GOF on F^2	1.205	1.061	0.955	1.133
Flack factor	N/A	0.03(4)	−0.04(3)	0.10(10)
*R*1, *wR*2 ($I > 2\sigma(I)$)[a]	0.0217, 0.0442	0.0302, 0.0715	0.0272, 0.0532	0.0443, 0.1050
*R*1, *wR*2 (all data)	0.0230, 0.0449	0.0308, 0.0723	0.0309, 0.0543	0.0456, 0.1057

[a] $R1 = \Sigma||F_o| - |F_c||/\Sigma|F_o|$, $wR2 = \{\Sigma w[(F_o)^2 - (F_c)^2]^2/\Sigma w[(F_o)^2]^2\}^{1/2}$.

agreement with the one determined from single crystal X-ray structural studies. IR data (KBr cm^{-1}): 3349 (m), 1614 (m), 982 (m), 962 (m), 807 (s), 783 (s), 749 (s), 663 (s), 490 (m), 456 (w), 422 (w).

Synthesis of $K(VO)_2O_2(IO_3)_3$. A mixture of K_2CO_3 (0.0552 g, 0.40 mmol), V_2O_5 (0.0920 g, 0.50 mmol), I_2O_5 (0.6686 g, 2.00 mmol), and H_2O (2.0 mL) was sealed in an autoclave equipped with a Teflon linear (20 mL) and heated at 160 °C for 4 days, followed by slow cooling to room temperature at a rate of 3 °C/h. The final pH value is about 0.5. The product was washed with water and ethanol and then dried in air. Large red brick-shaped crystals of $K(VO)_2O_2(IO_3)_3$ were obtained as a single phase in a yield of about 82% based on V. Its purity was confirmed by XRD studies (Figure S1, Supporting Information). It should be mentioned that $K(VO)_2O_2(IO_3)_3$ also has an excellent crystal growth habit. The product contains only one or several large crystals, which favors the growth of its large-size single crystals. The size of the single crystal has reached a maximum of 7 × 4 × 4 mm^3. The EDS elemental analyses on several single crystals of $K(VO)_2O_2(IO_3)_3$ gave an average molar ratio of K/V/I of 1.0: 2.1: 2.9, which is in good agreement with the one determined from single crystal X-ray structural studies. IR data (KBr cm^{-1}): 925 (m), 906 (m), 866 (m), 810 (m), 758 (s), 680 (s), 485 (m), 426 (m).

Single Crystal Structure Determination. Data collections for α-$KVO_2(IO_3)_2(H_2O)$, β-$KVO_2(IO_3)_2(H_2O)$, $K_4[(VO)(IO_3)_5]_2(HIO_3)(H_2O)_2\cdot H_2O$, and $K(VO)_2O_2(IO_3)_3$ were performed on a Rigaku Saturn 724 CCD diffractometer (for $K_4[(VO)(IO_3)_5]_2(HIO_3)(H_2O)_2\cdot H_2O$) or a Rigaku SCXMini CCD diffractometer (for the other three compounds) at 293(2) K, respectively, both equipped with a graphite-monochromated Mo−Kα radiation (λ = 0.71073 Å). The data sets were corrected for Lorentz and polarization factors as well as for absorption by multiscan method.[16] All four structures were solved by the direct methods and refined by full-matrix least-squares fitting on F^2 by SHELX-97.[17a] All four structures were checked for possible missing symmetry elements using PLATON.[17b] All nonhydrogen atoms were refined with anisotropic thermal parameters. Hydrogen atoms associated with water molecules and HIO_3 groups were located at geometrically calculated positions and refined with isotropic thermal parameters. Crystallographic data and structural refinements for the four compounds are summarized in Table 1. Important bond distances are listed in Table 2. More details on the crystallographic studies are given as Supporting Information.

Computational Descriptions. Single crystal structural data of our four compounds as well as $M[(VO)_2(IO_3)_3O_2]$ (M = Rb^+, Cs^+, NH_4^+) reported previously were used for the theoretical calculations. Band structures and density of states (DOS) were performed with the total-energy code CASTEP.[18] The total energy was calculated with density functional theory (DFT) using Perdew−Burke−Ernzerhof (PBE) generalized gradient approximation.[19] The interactions between the ionic cores and the electrons were described by the norm-conserving pseudopotential.[20] The following orbital electrons were treated as valence electrons: K, $3s^23p^64s^1$; Rb, $4s^24p^65s^1$; Cs, $5s^25p^66s^1$; V, $3d^34s^2$; I, $5s^25p^5$; O, $2s^22p^4$; N, $2s^22p^3$; and H, $1s^1$. The numbers of plane waves included in the basis sets were determined by a cutoff energy of 500 eV for all seven compounds, and the numerical integration of the Brillouin zone was performed using a Monkhorst−Pack *k*-point sampling of 3 × 3 × 1, 4 × 3 × 1, 3 × 3 × 2 for α-$KVO_2(IO_3)_2(H_2O)$, β-$KVO_2(IO_3)_2(H_2O)$, $K_4[(VO)(IO_3)_5]_2(HIO_3)(H_2O)_2\cdot H_2O$, respectively, and 4 × 4 × 3 for $K(VO)_2O_2(IO_3)_3$ and $M[(VO)_2(IO_3)_3O_2]$ (M = Rb^+, Cs^+, NH_4^+). The other parameters and convergent criteria were the default values of CASTEP code.

The calculations of linear optical properties in terms of the complex dielectric function $\varepsilon(\omega) = \varepsilon_1(\omega) + i\varepsilon_2(\omega)$ were made. The imaginary part of the dielectric function ε_2 was given in the following equation:[21]

$$\varepsilon_2^{ij}(\omega) = \frac{8\pi^2\hbar^2e^2}{m^2V}\sum_k\sum_{cv}(f_c - f_v)\frac{p_{cv}^i(k)p_{vc}^j(k)}{E_{vc}^2}\delta[E_c(k) - E_v(k) - \hbar\omega] \quad (1)$$

The f_c and f_v represent the Fermi distribution functions of the conduction and valence bands, respectively. The term $p_{cv}^i(k)$ denotes the momentum matrix element transition from the energy level c of the conduction band to the level v of the valence band at a certain *k* point in the Brillouin zones, and *V* is the volume of the unit cell. The *m*, *e*, and ħ are the electron mass, charge, and Plank's constant, respectively.

The second-order optical properties were calculated based on momentum gauge formalism with the minimal-coupling interaction Hamiltonian and within the independent particle approximation.[22] The imaginary part of the frequency-dependent second-order susceptibility $\chi^{(2)}(2\omega,\omega,\omega)$ is obtained from the electronic band structures by using the expressions already given elsewhere.[23] Then use the

dx.doi.org/10.1021/ja200257a | J. Am. Chem. Soc. 2011, 133, 5561–5572

Table 2. Selected Bond Distances (Å) for the Four Compounds[a]

		α-$KVO_2(IO_3)_2(H_2O)$			
V(1)−O(1)	1.959(3)	V(1)−O(4)	2.174(3)	V(1)−O(5)#1	2.007(3)
V(1)−O(7)	1.628(3)	V(1)−O(8)	1.660(3)	V(1)−O(8)#2	2.186(3)
I(1)−O(1)	1.863(3)	I(1)−O(2)	1.780(3)	I(1)−O(3)	1.802(3)
I(2)−O(4)	1.819(3)	I(2)−O(5)	1.856(3)	I(2)−O(6)	1.779(3)
O(1W)···O(1)#3	2.788(4)	O(1W)···O(6)#4	2.784(4)		
		β-$KVO_2(IO_3)_2(H_2O)$			
V(1)−O(1)	1.955(5)	V(1)−O(4)	2.013(4)	V(1)−O(6)#1	2.027(5)
V(1)−O(7)	1.620(5)	V(1)−O(8)	1.615(5)	I(1)−O(1)	1.863(5)
I(1)−O(2)	1.787(5)	I(1)−O(3)	1.773(5)	I(2)−O(4)	1.835(4)
I(2)−O(5)	1.779(5)	I(2)−O(6)	1.839(5)	O(1W)···O(2)#2	2.747(7)
O(1W)···O(3)#3	2.804(7)	O(1W)···O(4)	2.812(7)		
		$K_4[(VO)(IO_3)_5]_2(HIO_3)(H_2O)_2\cdot H_2O$			
V(1)−O(1)	1.918(8)	V(1)−O(4)	1.894(8)	V(1)−O(7)	1.914(8)
V(1)−O(10)	1.893(8)	V(1)−O(13)	2.170(9)	V(1)−O(34)	1.587(9)
V(2)−O(16)	1.891(8)	V(2)−O(19)	1.915(7)	V(2)−O(22)	1.973(8)
V(2)−O(25)	1.895(8)	V(2)−O(28)	2.197(9)	V(2)−O(35)	1.591(9)
I(1)−O(1)	1.883(8)	I(1)−O(2)	1.804(8)	I(1)−O(3)	1.842(7)
I(2)−O(4)	1.897(8)	I(2)−O(5)	1.808(8)	I(2)−O(6)	1.817(8)
I(3)−O(7)	1.860(8)	I(3)−O(8)	1.786(7)	I(3)−O(9)	1.809(8)
I(4)−O(10)	1.893(9)	I(4)−O(11)	1.785(8)	I(4)−O(12)	1.783(8)
I(5)−O(13)	1.823(8)	I(5)−O(14)	1.815(9)	I(5)−O(15)	1.810(8)
I(6)−O(16)	1.885(8)	I(6)−O(17)	1.796(8)	I(6)−O(18)	1.801(9)
I(7)−O(19)	1.888(8)	I(7)−O(20)	1.812(8)	I(7)−O(21)	1.798(9)
I(8)−O(22)	1.860(8)	I(8)−O(23)	1.816(7)	I(8)−O(24)	1.790(8)
I(9)−O(25)	1.867(8)	I(9)−O(26)	1.789(8)	I(9)−O(27)	1.792(8)
I(10)−O(28)	1.820(8)	I(10)−O(29)	1.812(7)	I(10)−O(30)	1.798(9)
I(11)−O(31)	1.805(9)	I(11)−O(32)	1.873(9)	I(11)−O(33)	1.797(9)
O(2W)···O(3W)	2.656(13)	O(2W)···O(20)	2.761(13)	O(3W)···O(12)#1	2.829(11)
		$K(VO)_2O_2(IO_3)_3$			
V(1)−O(1)	1.984(10)	V(1)−O(3)	2.207(10)	V(1)−O(4)#1	1.949(9)
V(1)−O(6)	1.626(10)	V(1)−O(7)	1.880(7)	V(1)−O(8)	1.885(5)
I(1)−O(1)	1.840(9)	I(1)−O(1)#2	1.840(9)	I(1)−O(2)	1.801(15)
I(2)−O(3)	1.841(9)	I(2)−O(4)	1.856(8)	I(2)−O(5)	1.765(12)

[a] Symmetry transformations used to generate equivalent atoms: For α-$KVO_2(IO_3)_2(H_2O)$: #1 $-x+3/2, y+1/2, z$; #2 $-x+3/2, y-1/2, z$; #3 $x-1/2, -y+1/2, -z+1$; #4 $-x+2, -y, -z+1$. For β-$KVO_2(IO_3)_2(H_2O)$: #1 $x+1/2, -y+3/2, -z+1$; #2 $-x, y+1/2, -z+3/2$; #3 $x, y+1, z$. For $K_4[(VO)(IO_3)_5]_2(HIO_3)(H_2O)_2\cdot H_2O$: #1 $x, y+1, z-1$. For $K(VO)_2O_2(IO_3)_3$: #1 $-x+1, -y, z$; #2 $-x+1/2, y, z$.

Kramers−Kronig relations, as required by causality, to obtain the real part:

$$\chi'^{(2)}(-2\omega,\omega,\omega) = \frac{2}{\pi}P\int_0^\infty d\omega' \frac{\omega'\chi''^{(2)}(2\omega',\omega',\omega')}{\omega'^2-\omega^2} \qquad (2)$$

In the present study, the δ function in the expressions for $\chi^{(2)}(2\omega,\omega,\omega)$[23a−c] was approximated by a Gaussian function with Γ = 0.2 eV. Furthermore, to ensure that the real part calculated via Kramer−Kronig transformation (eq 2) is reliable, at least 300 empty bands were used in SHG calculation. In addition, because DFT-GGA fails to correctly predict the CB energies, so the CB energy should be corrected by adding a scissor operator, and meanwhile, the momentum matrix elements were also renormalized.[23a]

RESULTS AND DISCUSSION

Four new potassium vanadyl iodates, namely, α-$KVO_2(IO_3)_2(H_2O)$, β-$KVO_2(IO_3)_2(H_2O)$, $K_4[(VO)(IO_3)_5]_2(HIO_3)(H_2O)_2\cdot H_2O$, and $K(VO)_2O_2(IO_3)_3$, have been successfully synthesized hydrothermally under different reaction conditions (Figure 1). It should be noted that $K_4[(VO)(IO_3)_5]_2(HIO_3)(H_2O)_2\cdot H_2O$ and $K(VO)_2O_2(IO_3)_3$ were synthesized under the same reaction temperature but different molar ratios of reactants, and the other two compounds were synthesized under different temperatures and molar ratios. In addition, Bi_2O_3 is necessary for the preparation of β-$KVO_2(IO_3)_2(H_2O)$, otherwise, only unknown amorphous phase can be isolated. The structures of the four compounds feature three different types of 1D anionic chains and a 0D cluster unit, all of which are separated by K^+ cations.

Structure of α-$KVO_2(IO_3)_2(H_2O)$. α-$KVO_2(IO_3)_2(H_2O)$ exhibits novel 1D $[VO_2(IO_3)_2]^-$ anionic chains which are separated by K^+ cations and the water molecules (Figure 2a). Both the V^{5+} and I^{5+} cations are in asymmetric coordination environments attributed to SOJT effects. The V^{5+} cation is octahedrally coordinated by one terminal and two bridging oxo anions as well as three iodate groups in a unidentate fashion. The V−O

dx.doi.org/10.1021/ja200257a | J. Am. Chem. Soc. 2011, 133, 5561–5572

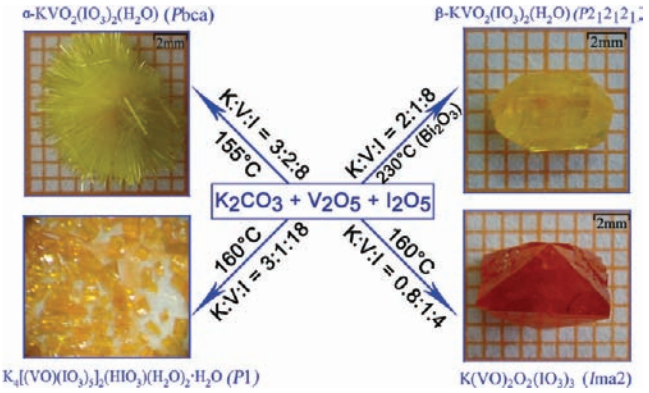

Figure 1. Synthetic routes and morphologies for α-$KVO_2(IO_3)_2$-(H_2O), β-$KVO_2(IO_3)_2(H_2O)$ ($6 \times 4 \times 2$ mm^3), $K_4[(VO)(IO_3)_5]_2$-$(HIO_3)(H_2O)_2 \cdot H_2O$, and $K(VO)_2O_2(IO_3)_3$ ($7 \times 4 \times 4$ mm^3).

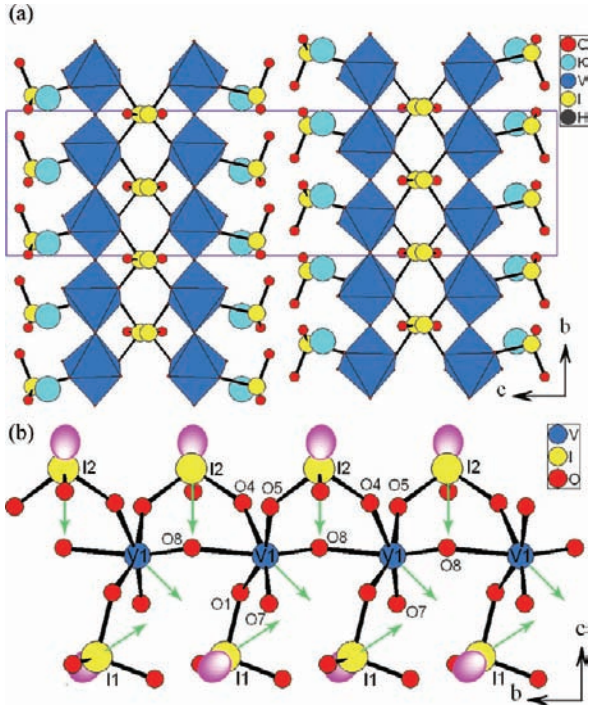

Figure 2. View of the structure of α-$KVO_2(IO_3)_2(H_2O)$ down the *a*-axis (a); a 1D $[VO_2(IO_3)_2]^-$ chain along the *b*-axis showing the lone pairs (purple ellipsoids) and local moments (green arrows) (b). VO_6 octahedra are shaded in blue and hydrogen atoms are omitted for clarity.

bond distances are: two long [2.174(3) and 2.186(3) Å], two normal [1.959(3) and 2.007(3) Å], and two short [1.628(3) and 1.660(3) Å], hence the VO_6 octahedron is distorted toward an edge (local C_2 direction) (Figure 2b). The magnitude of the out-of-center distortion (Δd) was calculated to be 1.16,[5] which is very strong and close to that in $LaVO_2(IO_3)_4 \cdot H_2O$ (Δd = 1.14).[13e] Neighboring VO_6 octahedra are corner sharing (O(8)) into a 1D linear vanadium oxide chain along the *b*-axis. I(1)O_3 groups are attached on one side of the chain unidentately, whereas I(2)O_3 groups are grafted in a bidentate bridging fashion into the chain on the other side (Figure 2b). Such a 1D anionic chain is related to that in $Ag_2VO_2(IO_3)_3$,[13d] however, the V(V) atoms in the 1D chain of $Ag_2VO_2(IO_3)_3$ are not aligned linearly but in a zigzag

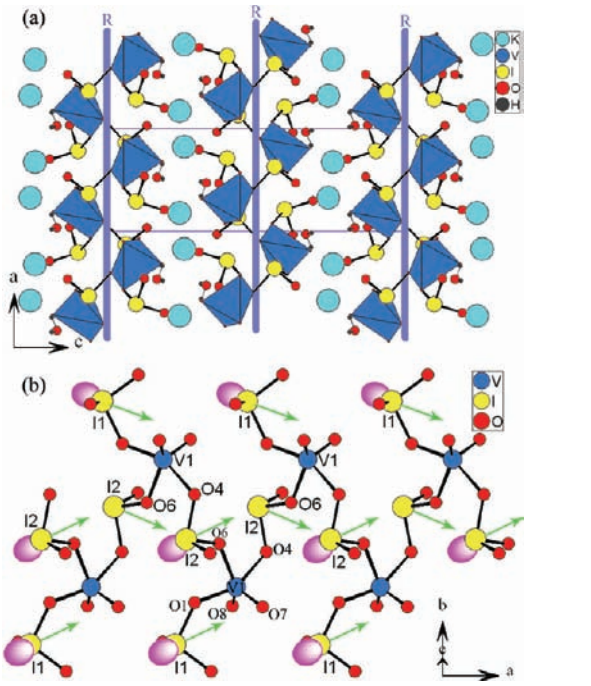

Figure 3. View of the structure of β-$KVO_2(IO_3)_2(H_2O)$ down the *b*-axis (a); a 1D $[VO_2(IO_3)_2]^-$ right-handed helical chain along the *a*-axis showing the lone pairs (purple ellipsoids) and local moments (green arrows) (b). VO_5 polyhedra are shaded in blue.

chain fashion. It should be also mentioned that such an 1D anionic chain is different from the one in $KVO_2(IO_3)_2$, though their chemical compositions are almost identical.[10b] The V^{5+} cation in $KVO_2(IO_3)_2$ is five-coordinated in a trigonal bipyramidal geometry, and these VO_5 polyhedra are not directly interconnected but bridged by iodate groups.

The I^{5+} cation is asymmetrically coordinated by three oxygen atoms in a distorted trigonal pyramidal environment as a result of its stereoactive lone pair. The I−O bond distances fall in the range of 1.779(3)−1.863(3) Å, which are comparable to those previously reported for other metal iodates.[10−13] The K^+ cation is surrounded by seven oxygen atoms from one O^{2-} anion, two water molecules, and four IO_3 groups in a pentagonal bipyramidal geometry, the K−O bond distances range from 2.689(3) to 3.213(4) Å. Bond valence calculations gave total bond valences of 1.03 for K, 5.04 for V, 4.96 and 5.01 for I,[24] indicating that the K, V, and I atoms are in an oxidation of +1, +5, and +5, respectively. It should be noted that the water molecule (O1W) is also involved in the hydrogen bonding with O(1) and O(6) [(2.788(4) and 2.784(4) Å].

Although each $[VO_2(IO_3)_2]^-$ chain is polar, there is no macroscopic polarization for the 3D network, since the polarizations of neighboring chains canceled each other due to the centrosymmetric space group (*Pbca*) (Figure 2a and b).

Structure of β-$KVO_2(IO_3)_2(H_2O)$. β-$KVO_2(IO_3)_2(H_2O)$ crystallizes in the chiral space group $P2_12_12_1$, and its structure contains right-handed helical chains of 1D $[VO_2(IO_3)_2]^-$ anions along the *a*-axis, which are separated by K^+ cations and the water molecules (Figure 3a). The V^{5+} cation is in a strongly distorted trigonal bipyramidal geometry and bonded to two terminal oxygen anions and three unidentate iodate groups, resulting in two short [1.615(5) and 1.620(5) Å] and three long [1.955(5), 2.013(4), and 2.027(5) Å] V−O bonds. Neighboring VO_5

dx.doi.org/10.1021/ja200257a |J. Am. Chem. Soc. 2011, 133, 5561–5572

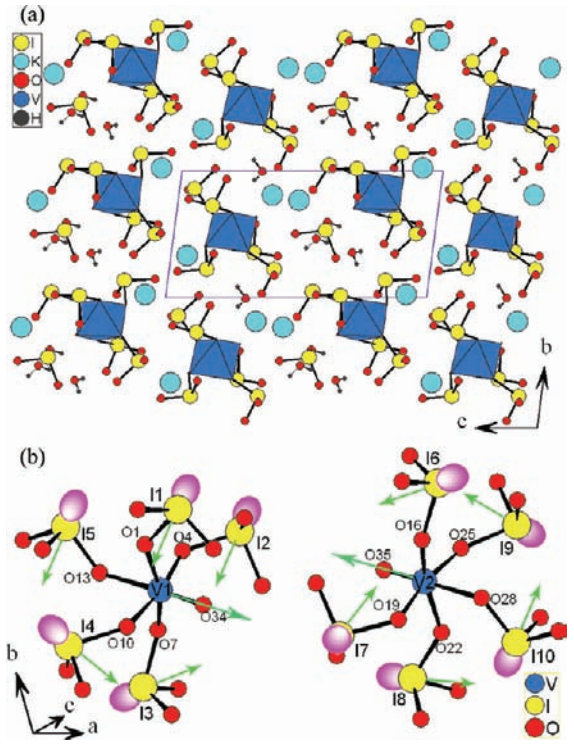

Figure 4. View of the structure of $K_4[(VO)(IO_3)_5]_2(HIO_3)(H_2O)_2 \cdot H_2O$ down the *a*-axis (a); two 0D $[(VO)(IO_3)_5]^{2-}$ anions in the asymmetric unit showing the lone pairs (purple ellipsoids) and local moments (green arrows) (b). VO_6 octahedra are shaded in blue.

polyhedra are further bridged by $I(2)O_3$ groups into a 1D right-handed helical chain along the *a*-axis. The $I(1)O_3$ groups are attached unidentately on both sides of the helical chain (Figure 3b). Such chain is similar to that in $NaVO_2(IO_3)_2(H_2O)$ but very different from that in α-$KVO_2(IO_3)_2(H_2O)$.[12b] Within the helical chain, the V^{5+} cations are arranged in a unusual zigzag manner rather than linearly in $KVO_2(IO_3)_2$[10b] and α-$KVO_2(IO_3)_2(H_2O)$. The V···V separation between the first and the third V atom of 5.808(1) Å is even much shorter than that between two neighboring ones bridged by an iodate group (6.032(1) Å) and slightly longer than that in $NaVO_2(IO_3)_2(H_2O)$[12b] (5.215(1) Å).

Both I^{5+} cations in the asymmetric unit are coordinated by three oxygen atoms in a distorted trigonal pyramidal environment, with the I−O bond distances ranging from 1.773(5) to 1.863(5) Å. The K^+ cation is in a square antiprismatic coordination environment composed of two terminal O^{2-} anions, one water molecule and five iodate groups. The K−O bond distances in the range of 2.703(5)−3.363(6) Å. Bond valence calculations gave total bond valences of 1.00 for K, 5.08 for V, and 5.10 and 4.96 for I, indicating that the K, V, and I atoms are in an oxidation of +1, +5, and +5, respectively.[24] H-bonding interactions are also present between water molecule and iodate groups [O(1W)···O(3) 2.804(7) Å and O(1W)···O(4) 2.812(7) Å].

Within the $[VO_2(IO_3)_2]^-$ helical chain, all of the lone pairs of the IO_3 groups are almost aligned in the same direction, producing a large macroscopic dipole moment toward the *a*-axis (Figure 3b). Different from those in $NaVO_2(IO_3)_2(H_2O)$,[12b] the large polarizations from two neighboring helical chains in β-$KVO_2(IO_3)_2(H_2O)$ mostly canceled each other (Figure 3a), resulting in only small macroscopic polarizations for the 3D

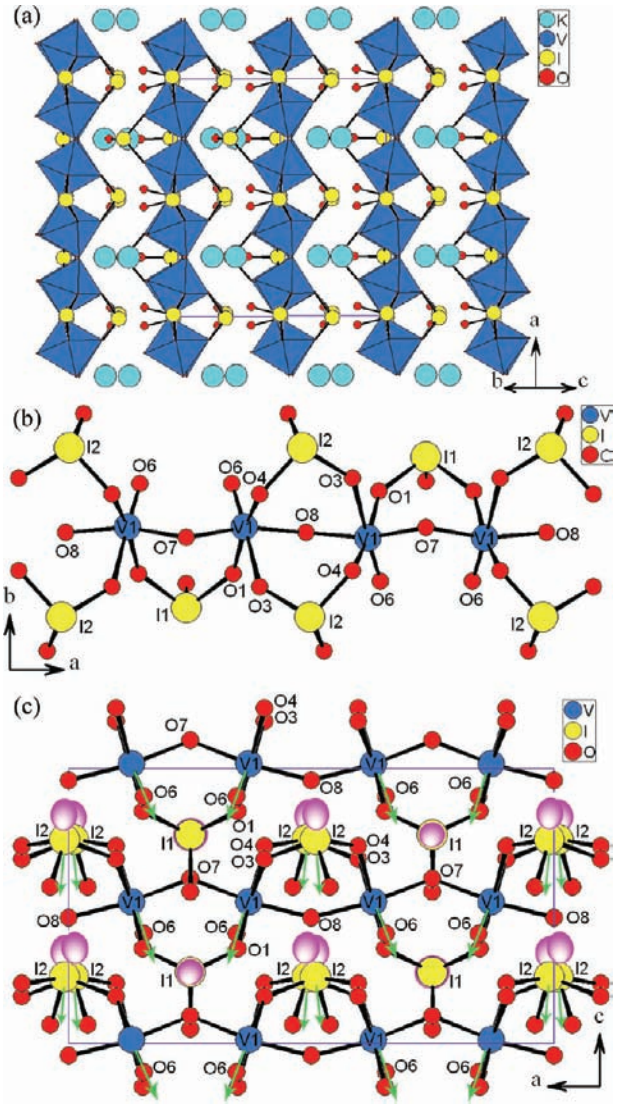

Figure 5. View of the structure of $K(VO)_2O_2(IO_3)_3$ (a); a $[(VO)_2O_2(IO_3)_3]^-$ chain along the *a*-axis (b); 1D $[(VO)_2O_2(IO_3)_3]^-$ chains along the *a*-axis showing the lone pairs (purple ellipsoids) and local moments (green arrows) (c). VO_6 octahedra are shaded in blue.

structure, which is confirmed by a very weak SHG response as will be discussed later.

Structure of $K_4[(VO)(IO_3)_5]_2(HIO_3)(H_2O)_2 \cdot H_2O$. It crystallizes in the polar space group *P*1, and its structure contains novel 0D $[(VO)(IO_3)_5]^{2-}$ anionic units composed of one VO_6 octahedron linked with five IO_3 groups and one terminal O^{2-} anion. The K^+ cations, water molecules, and HIO_3 groups are located between these 0D units (Figure 4a, 4b). So far only two 0D vanadium iodate anions have been reported, including $[VO_2(IO_3)_4]^{3-}$ and $[(V^{IV}O)(IO_3)_5]^{3-}$ units.[13b,e] Such 0D $[(VO)(IO_3)_5]^{2-}$ unit is different from the 0D $[(V^{IV}O)(IO_3)_5]^{3-}$ unit in $LaVO(IO_3)_5$,[13e] in the different charges for the vanadium atom and space arrangements for the five IO_3 groups, though their chemical compositions are similar.

The asymmetric unit contains 4 K^+, 2 V^{5+}, and 11 I^{5+} ions. Both V^{5+} cations undergo intraoctahedral distortion toward the terminal oxo anions, that is, a corner (C_4) distortion, exhibiting one short [1.587(9) or 1.591(9) Å], one long [2.170(9) or

dx.doi.org/10.1021/ja200257a |*J. Am. Chem. Soc.* 2011, 133, 5561–5572

2.197(9) Å], and four normal [1.893(8)−1.918(8) or 1.891(8)−1.973(8) Å] V−O bonds (Figure 4b). The magnitude of the out-of-center distortion (Δd) for $V(1)O_6$ and $V(2)O_6$ are estimated to be 0.59 and 0.71,[5] respectively, which are similar to that in $LaVO(IO_3)_5$ ($\Delta d = 0.67$)[13e] but much smaller than that in α-$KVO_2(IO_3)_2(H_2O)$. All I^{5+} cations are asymmetrically coordinated by three oxygen atoms in a distorted trigonal pyramidal environment with the I−O bond distances ranging from 1.783(8) to 1.897(8) Å. Both $K(1)^+$ and $K(2)^+$ cations are in a square antiprismatic coordination environment coordinated by eight iodate groups in a unidentate fashion. K(3) cation is surrounded by nine oxygen atoms from one oxo anion, one water molecule, one HIO_3, and four IO_3 groups (two of them in a bidentate chelating fashion) in a tricapped trigonal prism geometry, whereas K(4) cation is seven-coordinated with a pentagonal bipyramidal geometry composed of seven oxygen atoms from one O^{2-} anion, two water molecules, one HIO_3, and three IO_3 groups all in a unidentate fashion. The K−O bond distances fall in the range of 2.691(9)−3.202(8) Å. Bond valence calculations gave total bond valences of 0.91−1.28 for K, 5.06−5.20 for V, and 4.64−5.06 for I,[24] indicating that the K, V, and I atoms are in an oxidation of +1, +5, and +5, respectively. There are also extensive H-bonding interactions among coordinated and noncoordinated water molecules as well as IO_3 groups [O(2W)···O(20) 2.76(1) Å; O(3W)···O(12) 2.83(1) Å; O(2W)···O(3W) 2.66(1) Å].

As shown in Figure 4b, both 0D $[(VO)(IO_3)_5]^{2-}$ units in the asymmetric unit are polar. However, the polarizations of VO_6 and IO_3 groups from the two 0D units are toward almost opposite directions, resulting in largely cancellation of the local dipole moments, which is also confirmed by a very weak SHG response as will be discussed later.

Structure of $K(VO)_2O_2(IO_3)_3$. It is isostructural with $M[(VO)_2(IO_3)_3O_2]$ (M = Rb^+, Cs^+, NH_4^+) with a polar space group *Ima*2.[10b] Its structure contains a 1D $[(VO)_2O_2(IO_3)_3]^-$ anionic chain along the *a*-axis with the K^+ cations acting as spacers (Figure 5a and b). The asymmetric unit contains one V^{5+} and one I^{5+} cations in the general positions and one K^+ and one I^{5+} cations on a mirror plane. Both the V^{5+} and I^{5+} cations are in asymmetric coordination environments attributed to SOJT effects. The V^{5+} cation is distorted toward a corner (local C_4 direction), resulting in one long [2.21(1) Å], one short [1.63(1) Å], and four normal [1.880(7)−1.98(1) Å] V−O bonds (Figure 5b). The magnitude of the out-of-center distortion (Δd) was calculated to be a moderate value 0.62,[5] which is very close to that in $K_4[(VO)(IO_3)_5]_2(HIO_3)(H_2O)_2\cdot H_2O$ but much smaller than that in α-$KVO_2(IO_3)_2(H_2O)$. Neighboring VO_6 octahedra are corner-sharing bridging oxo anions into a 1D vanadium oxide chain along the *a*-axis. Within the chain, each pair of VO_6 octahedra is further bridged by one or two iodate anions alternatively (Figure 5b).

All I^{5+} cations in the asymmetric unit are coordinated by three oxygen atoms in a distorted trigonal-pyramidal geometry with the I−O bond distances falling in the normal range of 1.765(12) to 1.856(8) Å. The K^+ cation is eight-coordinated by three oxo anions and five unidentate iodate groups in a square antiprismatic geometry with the K−O bond distances in the range of 2.72(2) to 3.27(2) Å. Bond valence calculations gave total bond valences of 0.81 for K, 4.85 for V, 4.83 and 4.94 for I, respectively,[24] indicating that the K, V and I atoms are in an oxidation of +1, +5 and +5, respectively.

Within a $[(VO)_2O_2(IO_3)_3]^-$ chain, the lone pairs on the neighboring $I(1)O_3$ groups are nearly orientated toward opposite directions, which makes the polarizations of $I(1)O_3$ groups canceled out. However, all the lone pairs on $I(2)O_3$ groups are almost aligned in the same direction, so did the polarizations of VO_6 octahedra (Figure 5c). Hence, the polarizations associated with $I(2)O_3$ and VO_6 polyhedra constructively add, resulting in a large macroscopic polarization, which is confirmed by the SHG measurements discussed later.

TGA and DTA. Thermogravimetric analysis (TGA) studies indicate that α-$KVO_2(IO_3)_2(H_2O)$, β-$KVO_2(IO_3)_2(H_2O)$, $K_4[(VO)(IO_3)_5]_2(HIO_3)(H_2O)_2\cdot H_2O$, and $K(VO)_2O_2(IO_3)_3$ are thermally stable up to about 115, 200, 170, and 335 °C, respectively. Then $K(VO)_2O_2(IO_3)_3$ displays one step of weight loss, whereas the other three compounds each displays two main steps of weight losses (Figure 6). For $K(VO)_2O_2(IO_3)_3$, the weight loss in the temperature range 335−440 °C corresponds to the release of 1.5 I_2 and 3.75 O_2 per formula unit, which is in agreement with the two endothermic peaks observed at 342 and 406 °C in the differential thermal analysis (DTA) diagram. The residuals at 900 °C should be $K_3V_5O_{14}$ and $K_{1.11}V_3O_8$ based on powder XRD studies (Figure S2d, Supporting Information). The corresponding observed total weight loss of 68.3% is close to the calculated ones (68.6%).

For α-$KVO_2(IO_3)_2(H_2O)$, β-$KVO_2(IO_3)_2(H_2O)$, and $K_4[(VO)(IO_3)_5]_2(HIO_3)(H_2O)_2\cdot H_2O$, the weight losses in the temperature ranges 115−250, 200−235, 170−235 °C correspond to the release of 1.0 H_2O, 1.0 H_2O, and 3.0 H_2O molecules per formula unit, respectively, which are in agreement with the endothermic peaks at 138 and 235 °C, 213 °C, and 207 °C, respectively, in their DTA diagrams. The observed weight losses of 3.7, 3.6, and 2.4%, respectively, for α-$KVO_2(IO_3)_2(H_2O)$, β-$KVO_2(IO_3)_2(H_2O)$, and $K_4[(VO)(IO_3)_5]_2(HIO_3)(H_2O)_2\cdot H_2O$ are very close to the calculated ones (3.68, 3.68, and 2.38%). After dehydration, α-$KVO_2(IO_3)_2(H_2O)$ and $K_4[(VO)(IO_3)_5]_2(HIO_3)(H_2O)_2\cdot H_2O$ become amorphous, whereas β-$KVO_2(IO_3)_2(H_2O)$ has been converted to $KVO_2(IO_3)_2$[10b] as confirmed by powder XRD studies (Figure S2b, Supporting Information).

The second weight loss (360−530, 360−550, and 310−570 °C, respectively, for α-$KVO_2(IO_3)_2(H_2O)$, β-$KVO_2(IO_3)_2(H_2O)$, and $K_4[(VO)(IO_3)_5]_2(HIO_3)(H_2O)_2\cdot H_2O$) corresponds to further decomposition for each compound, which is consistent with the endothermic peaks at 368 and 423 °C for α-$KVO_2(IO_3)_2(H_2O)$, 363 and 416 °C for β-$KVO_2(IO_3)_2(H_2O)$, and 425, 500, and 574 °C for $K_4[(VO)(IO_3)_5]_2(HIO_3)(H_2O)_2\cdot H_2O$ in the DTA diagrams. The residuals at 900 °C should be KVO_3 for α-$KVO_2(IO_3)_2(H_2O)$ and β-$KVO_2(IO_3)_2(H_2O)$, KVO_3 and an unknown phase for $K_4[(VO)(IO_3)_5]_2(HIO_3)(H_2O)_2\cdot H_2O$ based on powder XRD studies (Figure S2, Supporting Information). Assuming that the unknown phase is composed of the oxides of potassium and vanadium, as in other three compounds, the total weight losses of 71.34, 71.76, and 84.08% for α-$KVO_2(IO_3)_2(H_2O)$, β-$KVO_2(IO_3)_2(H_2O)$, and $K_4[(VO)(IO_3)_5]_2(HIO_3)(H_2O)_2\cdot H_2O$ match well with the calculated values of 71.82, 71.82, and 83.68%, respectively.

Optical Properties. IR spectra indicate that $K(VO)_2O_2(IO_3)_3$ is transparent in the range of 4000−1000 cm^{-1} (2.5−10 μm), whereas the other three compounds show a few absorption bands associated with the water molecules (Figure S3, Supporting Information). The IR absorption bands at 866−982 and 421−827 cm^{-1} can be assigned to V−O and I−O vibrations, respectively. For the three compounds containing water

dx.doi.org/10.1021/ja200257a |*J. Am. Chem. Soc.* 2011, 133, 5561–5572

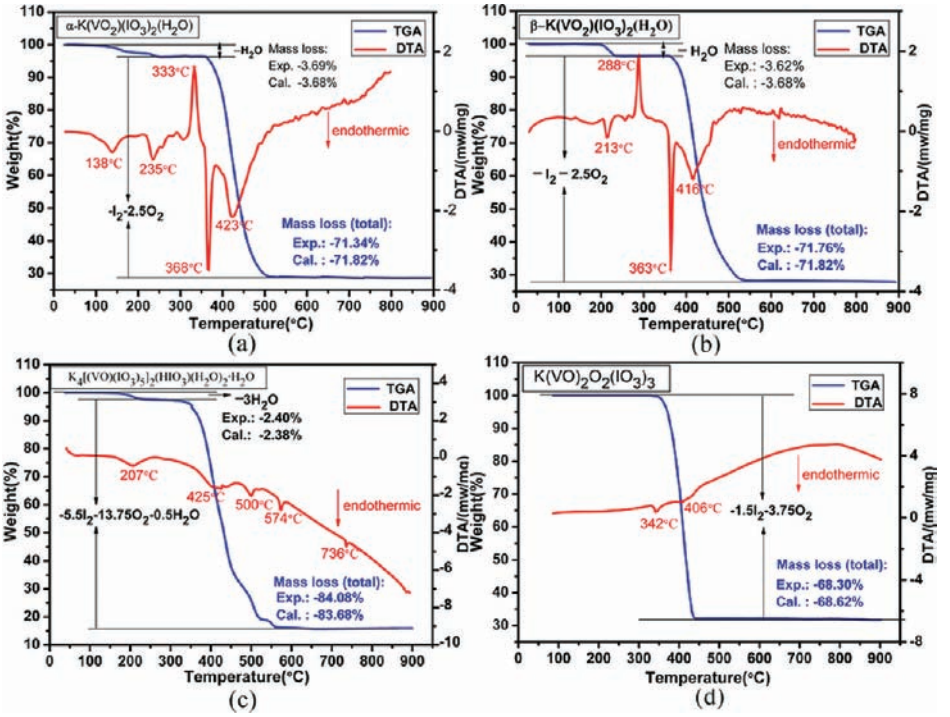

Figure 6. TGA and DTA curves for α-$KVO_2(IO_3)_2(H_2O)$ (a), β-$KVO_2(IO_3)_2(H_2O)$ (b), $K_4[(VO)(IO_3)_5]_2(HIO_3)(H_2O)_2\cdot H_2O$ (c), and $K(VO)_2O_2(IO_3)_3$ (d).

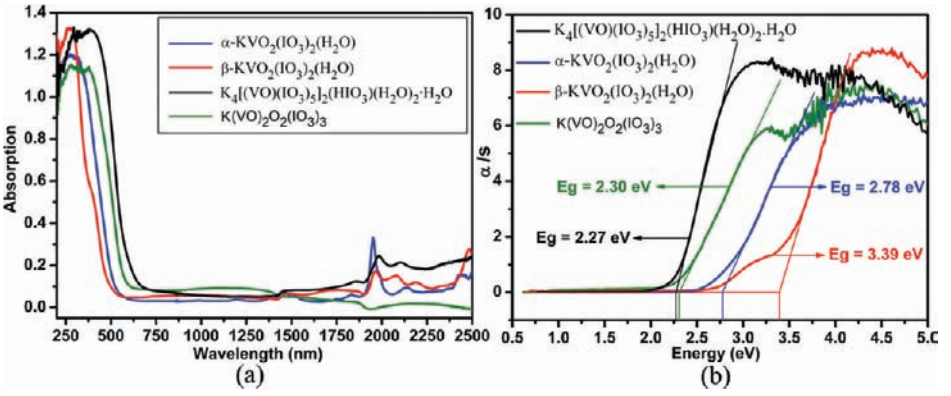

Figure 7. UV absorption spectra (a) and optical diffuse reflectance spectra (b) for the four compounds.

molecules, the broad bands centered at 3535, 3426, 3137, and 3349 cm^{-1} and 1617, 1623, and 1614 cm^{-1} can be assigned to stretching and bending modes of the water molecules, respectively. These assignments are in consistent with those previously reported.[10,13,25,26]

UV absorption spectra of all four compounds show little absorption in the range of 650−2500 nm (0.65−2.5 μm) (Figure 7a). Hence, $K(VO)_2O_2(IO_3)_3$ is transparent in the range of 0.65−10 μm (Figure S3, Supporting Information, Figure 7a), responding to visible, near, and middle IR regions. The other three compounds show a few absorption bands associated with the water molecules as mentioned earlier. Optical diffuse reflectance spectrum measurements indicate that α-$KVO_2(IO_3)_2(H_2O)$, β-$KVO_2(IO_3)_2(H_2O)$, $K_4[(VO)(IO_3)_5]_2(HIO_3)(H_2O)_2\cdot H_2O$, and $K(VO)_2O_2(IO_3)_3$ are wide band gap semiconductors with optical band gaps of 2.78, 3.39, 2.27, and 2.30 eV, respectively (Figure 7b).

Second-Harmonic Generation (SHG) Properties. Since β-$KVO_2(IO_3)_2(H_2O)$, $K_4[(VO)(IO_3)_5]_2(HIO_3)(H_2O)_2\cdot H_2O$, and $K(VO)_2O_2(IO_3)_3$ crystallized in noncentrosymmetric space groups, it is worthy to study their SHG properties. SHG measurements on a 2.05 μm Q-switch laser with the sieved powder samples revealed that β-$KVO_2(IO_3)_2(H_2O)$ and $K_4[(VO)(IO_3)_5]_2(HIO_3)(H_2O)_2\cdot H_2O$ display very weak SHG signals, whereas $K(VO)_2O_2(IO_3)_3$ shows a very strong SHG response of about 3.6 × KTP ($KTiOPO_4$) and is also phase-matchable (Figure 8). Based on structural data, it is expected that the very weak SHG responses for β-$KVO_2(IO_3)_2(H_2O)$ and $K_4[(VO)(IO_3)_5]_2(HIO_3)(H_2O)_2\cdot H_2O$ may be mainly caused by the partial cancellation of the local dipole moments associate with VO_x (x = 5, 6) and IO_3 groups. The very strong SHG response for $K(VO)_2O_2(IO_3)_3$ mainly stems from the synergistic effect of two types of NLO-active units (IO_3 and VO_6), that is,

dx.doi.org/10.1021/ja200257a |J. Am. Chem. Soc. 2011, 133, 5561–5572

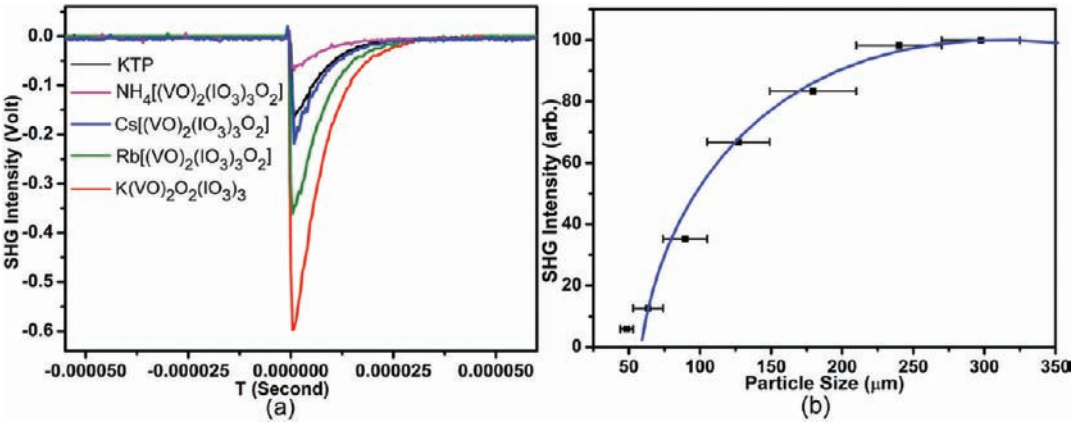

Figure 8. Oscilloscope traces of the SHG signals for the powders (270−325 μm) of KTP, $K(VO)_2O_2(IO_3)_3$ and $M[(VO)_2(IO_3)_3O_2]$ ($M = Rb^+$, Cs^+, NH_4^+) (a) and the phase-matching curve for $K(VO)_2O_2(IO_3)_3$(b). The curve drawn is to guide the eye and not a fit to the data.

the polarizations associated with all IO_3 and VO_6 polyhedra constructively add, producing a very large net dipole moment.

To better understand the magnitude and direction of the dipole moments, the local dipole moments for the IO_3 and VO_6 or VO_5 polyhedra and the net dipole moment within a unit cell for all four compounds were calculated by using a method reported earlier.[13e,25,27] With the lone-pair polyhedra, the lone-pair is given a charge of −2 and is localized 1.23 Å from the I(V) cations.[28] The dipole moment calculations for four compounds resulted in values of 13.23−16.59 D (D = Debyes) for IO_3, 3.05 D for VO_5 and 5.34−7.64 D for VO_6 polyhedra (Table S1, Supporting Information), which is consistent with previously reported values.[13e,27] For α-$KVO_2(IO_3)_2(H_2O)$, the polarizations of neighboring chains cancel out completely due to the centrosymmetric space group (see Figure 2) and the net dipole moment for a unit cell is 0 D. For β-$KVO_2(IO_3)_2(H_2O)$, the *x*, *y*, and *z*-component of the polarizations from four $I(1)O_3$ polyhedra within a unit cell are 2 × (±9.85 D), 2 × (±4.94 D) and 2 × (±9.10 D), respectively. Hence, the polarizations from the four $I(1)O_3$ canceled out completely in each direction. Such cancellations are also observed for the $I(2)O_3$ and $V(1)O_5$ polyhedra (see Figure 3 and Table S1, Supporting Information). Thus, the net dipole moment of a unit cell is 0 D. For $K_4[(VO)(IO_3)_5]_2(HIO_3)(H_2O)_2\cdot H_2O$, the *x*, *y*, and *z*-component of the polarizations from $V(1)O_6$ and $V(2)O_6$ are almost equal in magnitude but opposite in direction. Hence, the polarizations from the two VO_6 polyhedra almost canceled each other. As for the 11 IO_3 polyhedra in a unit cell, the main contributions of the *x*-component of the polarizations come from $I(x)O_3$ (x = 1, 2, 5, 6, 9, 11) which are partially canceled by those of $I(x)O_3$ (x = 3, 4, 7, 8, 10) (see Figure 4 and Table S1, Supporting Information). Similarly, the *y*-component of the polarizations from $I(x)O_3$ (x = 1−5, 8, 11) are partially canceled by those of $I(x)O_3$ (x = 6, 7, 9, 10) and the *z*-component of the polarizations from $I(x)O_3$ (x = 2, 3, 8, 10, 11) are partially canceled by those of $I(x)O_3$ (x = 1, 4−7, 9). The net dipole moment of a unit cell was calculated to be a relative small value of 33.62 D. For $K(VO)_2O_2(IO_3)_3$, the *x*, *y*, and *z*-component of the polarizations from four $I(1)O_3$ polyhedra in a unit cell are 4 × (0 D), 2 × (±14.53 D) and 4 × (2.67 D), respectively. Hence, the *y*-component of the polarizations from four $I(1)O_3$ polyhedra canceled out completely, and only the *z*-component of their polarizations constructively adds to a value of 10.68 D. As for the eight $I(2)O_3$ polyhedra in a unit cell, the *x*, *y*, and *z*-component of their polarizations are 4 × (±1.08 D), 4 × (±4.35 D), and 8 × (12.59 D), respectively. Thus the *x* and *y*-component of their polarizations canceled out completely, whereas those of the *z*-components constructively add to a large value of 100.72 D. Similarly, the *x* and *y*-component of the polarizations associated with all eight $V(1)O_6$ polyhedra in a unit cell canceled each other out, and the *z*-component of their polarizations constructively adds to a value of 18.08 D (see Figure 5 and Table S1, Supporting Information) The *z*-component of all $I(1)O_3$, $I(2)O_3$, and $V(1)O_6$ constructively adds to produce a very large net dipole moment of 129.48 D along the *c*-axis. These results are in agreement with those of SHG measurements.

It is reported that the cesium phase of the isostructural $M[(VO)_2(IO_3)_3O_2]$ ($M = Rb^+$, Cs^+, NH_4^+) displays a SHG response of 500 × α-SiO_2,[10b] and the SHG properties of the other two phases were not mentioned. For comparison with our compounds, the SHG measurements of these three compounds were also performed under the same conditions. Results indicate SHG responses of 2.2, 1.3, and 0.4 × KTP, respectively, for the rubidium, cesium, and ammonium phases (Figure 8a). It is then concluded that the SHG responses of the four isostructural compounds follow a sequence of K > Rb > Cs > NH_4. This is largely in agreement with results from the theoretical calculations on the SHG susceptibility coefficients for the four isostructural compounds as will be discussed later. It is expected that the weak SHG responses for β-$KVO_2(IO_3)_2(H_2O)$ and $K_4[(VO)(IO_3)_5]_2(HIO_3)(H_2O)_2\cdot H_2O$ should originate from not only the partial cancellation of the local dipole moments associate with VO_x (x = 5, 6) and IO_3 groups but also the absorption bands near 2.0 μm caused by the water molecules. For the ammonium phase, the absorption bands near 2.0 μm associated with the N−H vibration may be also responsible for its relative weak SHG response.

Ferroelectric Properties. The ferroelectric properties of $K_4[(VO)(IO_3)_5]_2(HIO_3)(H_2O)_2\cdot H_2O$ and $K(VO)_2O_2(IO_3)_3$ were investigated because they crystallized in polar point groups (1 and *mm*2) required for ferroelectric behavior. Ferroelectric measurements on a pellet (5 mm diameter and 0.8 mm thick) for $K_4[(VO)(IO_3)_5]_2(HIO_3)(H_2O)_2\cdot H_2O$ and on a single crystal with a size of 5.8 × 1.86 × 1.46 mm^3 in the direction of the *c*-axis for $K(VO)_2O_2(IO_3)_3$ revealed small remanent polarizations (Pr) of 0.27 and 0.045 $\mu C/cm^2$ respectively (Figure S6, Supporting

dx.doi.org/10.1021/ja200257a |*J. Am. Chem. Soc.* 2011, 133, 5561–5572

Information), hence the ferroelectric properties are negligible. It is unlikely that the dipole moments associated with the asymmetric IO_3 polyhedra can be reversible as reported by other groups.[11] Hence the polarization reversibility may be limited to the small contribution from the distorted VO_6 octahedra or derived from dielectric loss.

Hardness Measurements. The Vickers-hardness measurements were carried out with the crystals of β-$KVO_2(IO_3)_2(H_2O)$ and $K(VO)_2O_2(IO_3)_3$ on a 401 MVA Vickers hardness tester. The Vickers-hardness values of β-$KVO_2(IO_3)_2(H_2O)$ and $K(VO)_2O_2(IO_3)_3$ are 94 and 195 HV, respectively, about 2.5 and 3.0 in Mohs' scale, which allows easy polishing for the crystals.

Theoretical Calculations. To gain further insights on the electronic structures of four materials and optical properties of three NCS compounds, theoretical calculations based on DFT methods were performed by using the total-energy code CASTEP.[18] The SHG properties of the $M[(VO)_2(IO_3)_3O_2]$ (M = Rb^+, Cs^+, NH_4^+) were also calculated for comparison with that of the isostructural $K(VO)_2O_2(IO_3)_3$.

The dispersions of energy bands are presented in Figure S7, Supporting Information and the state energies (eV) of the lowest conduction band (L-CB) and the highest valence band (H-VB) of the compounds are listed in Table S2, Supporting Information. For α-$KVO_2(IO_3)_2(H_2O)$ and β-$KVO_2(IO_3)_2(H_2O)$, both the L-CBs and the H-VBs are located at the same point, with direct band gaps of 2.66 and 2.51 eV, respectively. For $K_4[(VO)(IO_3)_5]_2(HIO_3)(H_2O)_2\cdot H_2O$ and $K(VO)_2O_2(IO_3)_3$, the L-CBs and the H-VBs are located at different symmetry points, giving indirect band gaps of 2.00 and 1.67 eV. The calculated band gaps of the four materials are all somewhat smaller than the experimental values (2.78, 3.39, 2.27, and 2.30 eV, respectively). This is not surprising as it is well-known that the GGA does not accurately describe the eigenvalues of the electronic states, which often causes quantitative underestimation of band gaps for semiconductors and insulators.[29] Hence scissors were adopted during the optical property calculations for all compounds (Table S3, Supporting Information).

The bands can be assigned according to the total and partial DOS, as plotted in Figure S8, Supporting Information. All of the four compounds display very similar characteristics, thus, we only take α-$KVO_2(IO_3)_2(H_2O)$ as a representative to discuss the DOS in detail. The bottom-most VBs ranging from −27.0 to −26.5 eV are composed of K-3s states. The VBs between −20.5 and −15.0 eV are originated from O-2s and small amounts of I-5s, I-5p states, whereas the VBs between −11.5 and −8.0 eV arise from K-3p states mixing with a dash of O-2p and I-5s states. The Fermi level region, which accounts for most of the bonding character in a compound, falls in the range of −6.5 to 5.0 eV. It is obvious that O-2p states dominate the whole Fermi level region. In the regions of −6.5 to −4.0 and 2.5 to 5.0 eV, I-5p states overlap fully with O-2p, and in the regions of −4.0 to 5.0 eV, V-3d states also overlap well with O-2p, indicating the well-defined V−O coordination in vanadium oxide polyhedra and I−O covalent interactions.

Population analyses allow for a more quantitative bond analysis (Table S4, Supporting Information). The calculated bond orders of K−O and I−O bonds are 0.01−0.15 and 0.12−0.56 e respectively for all four compounds, indicating that the K−O bonds are ionic and the I−O bonds are more covalent in character. The V−O bonds in the four compounds can be divided into three types: V−O(−V) (only exist in α-$KVO_2(IO_3)_2(H_2O)$ and $K(VO)_2O_2(IO_3)_3$), V−O(terminal), and V−O(−I) (both exist in all compounds). The calculated bond orders of V−O(terminal), V−O(−V), and V−O(−I) are 0.90−0.94, 0.25−0.8, and 0.23−0.45 e, respectively, indicating the covalent character of these V−O bonds normally follow the order of V−O(terminal) > V−O(−V) > V−O(−I).

Furthermore, we also explored the linear and nonlinear optical properties of the NCS crystals. It is noticeable that all of the optical properties calculations of these compounds in this paper were based on their principal dielectric axis coordinate systems. For the triclinic crystal $K_4[(VO)(IO_3)_5]_2(HIO_3)(H_2O)_2\cdot H_2O$, optical permittivity tensor matrix was calculated and transformed to its diagonal form (i.e., the principal axes transformation), and the obtained angles between the crystallography axes (i.e., *a*, *b* and *c*) and the principal dielectric axes (i.e., *x*, *y*, and *z*) were listed in Table S5, Supporting Information.

The linear optical response properties of three NCS compounds were examined through calculating the complex dielectric function $\varepsilon(\omega) = \varepsilon_1(\omega) + i\varepsilon_2(\omega)$. Its imaginary part ($\varepsilon_2(\omega)$) can be used to describe the real transitions between the occupied and unoccupied electronic states. The imaginary parts of the frequency-dependent dielectric functions of the compounds show anisotropic along three dielectric axis directions (Figures S9 a−c, Supporting Information). The curves of the averaged imaginary parts and real parts of dielectric functions were obtained by $\varepsilon^{ave} = (\varepsilon_x + \varepsilon_y + \varepsilon_z)/3$ (Figures S9 d−f, Supporting Information). The averaged imaginary parts reveal the strongest adsorption peaks of β-$KVO_2(IO_3)_2(H_2O)$, $K_4[(VO)(IO_3)_5]_2(HIO_3)(H_2O)_2\cdot H_2O$, and $K(VO)_2O_2(IO_3)_3$ are at 5.5, 4.9, and 4.9 eV, respectively, which can be mainly assigned to the electronic interband transitions from the O-2p to I-5p and V-3d states. The average static dielectric constant $\varepsilon(0)$ of β-$KVO_2(IO_3)_2(H_2O)$, $K_4[(VO)(IO_3)_5]_2(HIO_3)(H_2O)_2\cdot H_2O$, and $K(VO)_2O_2(IO_3)_3$ is 4.03, 4.66, and 5.58. The dispersion curves of refractive indices calculated by the formula $n^2(\omega) = \varepsilon(\omega)$ display strong anisotropy which arises from the anisotropy of the dielectric functions, $n^z > n^y > n_\infty$ for β-$KVO_2(IO_3)_2(H_2O)$, $n^z > n_\infty > n^y$ for $K_4[(VO)(IO_3)_5]_2(HIO_3)(H_2O)_2\cdot H_2O$, and $n^x > n^y > n^z$, but n^x is much larger than n^y and n^z for $K(VO)_2O_2(IO_3)_3$ (Figure S10, Supporting Information). The values of n^x, n^y, and n^z at 2 μm are calculated to be 1.945, 2.031, and 2.065 for β-$KVO_2(IO_3)_2(H_2O)$, 2.161, 2.123, and 2.236 for $K_4[(VO)(IO_3)_5]_2(HIO_3)(H_2O)_2\cdot H_2O$, and 2.638, 2.257, and 2.228 for $K(VO)_2O_2(IO_3)_3$, respectively.

Based on the space groups and the Kleinman symmetry, β-$KVO_2(IO_3)_2(H_2O)$, $K_4[(VO)(IO_3)_5]_2(HIO_3)(H_2O)_2\cdot H_2O$, and $K(VO)_2O_2(IO_3)_3$ has 1, 10, and 3 nonvanishing independent SHG coefficient tensors, respectively. The frequency-dependent SHG tensors of these compounds are plotted in Figure S11, Supporting Information. At the wavelength of 2 μm (0.62 eV), the highest tensors d_{14} for β-$KVO_2(IO_3)_2(H_2O)$, d_{34} for $K_4[(VO)(IO_3)_5]_2(HIO_3)(H_2O)_2\cdot H_2O$, and d_{15} for $K(VO)_2O_2(IO_3)_3$ are 1.72×10^{-9}, 8.69×10^{-9}, and 5.50×10^{-8} esu, respectively, which are in agreement with our experimental ones of weak SHG responses for the former two compounds and about 3.6 times that of KTP ($d_{24} = 1.8 \times 10^{-8}$ esu) for $K(VO)_2O_2(IO_3)_3$. The calculated SHG response curves of the Rb^+, Cs^+, and NH_4^+ phases isostructural with $K(VO)_2O_2(IO_3)_3$ are shown in Figure S12, Supporting Information. The highest tensor d_{15} is 5.17×10^{-8}, 4.30×10^{-8}, and 3.89×10^{-8} esu, respectively, for Rb^+, Cs^+, and NH_4^+ compounds. Therefore, the calculated SHG responses follow a sequence of K > Rb > Cs > NH_4, which is in agreement with the experimental ones.

dx.doi.org/10.1021/ja200257a |*J. Am. Chem. Soc.* 2011, 133, 5561–5572

CONCLUSIONS

In summary, four new potassium vanadyl iodates based on lone-pair-containing IO_3 and SOJT distorted VO_5 or VO_6 asymmetric units, namely, α-$KVO_2(IO_3)_2(H_2O)$ (*Pbca*), β-$KVO_2(IO_3)_2(H_2O)$ ($P2_12_12_1$), $K_4[(VO)(IO_3)_5]_2(HIO_3)(H_2O)_2 \cdot H_2O$ (*P*1), and $K(VO)_2O_2(IO_3)_3$ (*Ima*2) have been successfully synthesized by hydrothermal reactions under different conditions. Their structures feature three different types of 1D anionic chains and a 0D anionic unit. The differences between these four types of anionic structures are mainly caused by the different coordination geometries of the vanadium(V) cations as well as the coordination fashions of the iodate anions. Three of them are NCS, and $K(VO)_2O_2(IO_3)_3$ displays a very strong SHG efficiency of about 3.6 × KTP due to the synergistic effect of two types of NLO-active units (IO_3 and VO_6). The SHG response for $K(VO)_2O_2(IO_3)_3$ is the largest among the $M[(VO)_2(IO_3)_3O_2]$ ($M = K^+$, Rb^+, Cs^+, NH_4^+) family based on our experimental measurements as well as theoretical calculations. Furthermore, $K(VO)_2O_2(IO_3)_3$ is phase matchable and also has high thermal stability, a wide transparent region as well as moderate hardness. On the other hand, it is very important that the excellent growth habit of $K(VO)_2O_2(IO_3)_3$ favors the growth of its large-size crystals. Based on these intriguing overall properties, it is concluded that $K(VO)_2O_2(IO_3)_3$ is a promising candidate for second-order NLO materials used in the visible, near, and mid-IR regions. Our future research efforts will be devoted to growing larger size $K(VO)_2O_2(IO_3)_3$ crystals with better quality to further study its optical properties such as transparent range, refractive index, the Sellmeier equations, and laser damage threshold.

ASSOCIATED CONTENT

Supporting Information. X-ray crystallographic files in CIF format, simulated and experimental XRD patterns, IR, UV absorption and optical diffuse reflectance spectra, and ferroelectric data. This material is available free of charge via the Internet at http://pubs.acs.org.

AUTHOR INFORMATION

Corresponding Author
mjg@fjirsm.ac.cn

ACKNOWLEDGMENT

This work was supported by the National Natural Science Foundation of China (nos. 20731006, 20825104, 21003127, and 20821061). We thank Prof. Xi-Fa Long and Dr. Chao He for their kind help with the ferroelectric measurements.

REFERENCES

(1) (a) Chen, C.; Liu, G. *Annu. Rev. Mater. Sci.* **1986**, *16*, 203. (b) Halasyamani, P. S.; Poeppelmeier, K. R. *Chem. Mater.* **1998**, *10*, 2753. (c) Ok, K. M.; Halasyamani, P. S. *Chem. Soc. Rev.* **2006**, *35*, 710.

(2) (a) Becker, P. *Adv. Mater.* **1998**, *10*, 979. (b) Chen, C. T.; Wang, Y. B.; Wu, B. C.; Wu, K. C.; Zeng, W. L.; Yu, L. H. *Nature* **1995**, *373*, 322. (c) Chen, C. T.; Wu, B. C.; Jiang, A. D.; You, G. M. *Sci. Sin., Ser B* **1984**, *14*, 598. (d) Hagerman, M. E.; Poeppelmeier, K. R. *Chem. Mater.* **1995**, *7*, 602. (e) Ballman, A. A.; Brown, H. *J. Cryst. Growth* **1967**, *1*, 311.

(3) (a) Dmitriev, V. G.; Gurzadyan, G. G.; Nikogosyan, D. N. *Handbook of Nonlinear Optical Crystals*; Springer: Berlin, Germany, 1991. (b) Boyd, G. D.; Buehler, E.; Storz, F. G. *Appl. Phys. Lett.* **1971**, *18*, 301. (c) Liao, J. H.; Marking, G. M.; Hsu, K. F.; Matsushita, Y.; Ewbank, M. D.; Borwick, R.; Cunningham, P.; Rosker, M. J.; Kanatzidis, M. G. *J. Am. Chem. Soc.* **2003**, *125*, 9484. (d) Zhang, Q.; Chung, I.; Jang, J. I.; Ketterson, J. B.; Kanatzidis, M. G. *J. Am. Chem. Soc.* **2009**, *131*, 9896.

(4) (a) Pan, S. L.; Smit, J. P.; Watkins, B.; Marvel, M. R.; Stern, C. L.; Poeppelmeier, K. R. *J. Am. Chem. Soc.* **2006**, *128*, 11631. (b) Zhang, W. L.; Cheng, W. D.; Zhang, H.; Geng, L.; Lin, C. S.; He, Z. Z. *J. Am. Chem. Soc.* **2010**, *132*, 1508. (c) Huang, Y. Z.; Wu, L. M.; Wu, X. T.; Li, L. H.; Chen, L.; Zhang, Y. F. *J. Am. Chem. Soc.* **2010**, *132*, 12788.

(5) Halasyamani, P. S. *Chem. Mater.* **2004**, *16*, 3586and references cited therein.

(6) (a) Ok, K. M.; Halasyamani, P. S. *Angew. Chem. In. Ed.* **2004**, *43*, 5489. (b) Phanon, D.; Gautier-Luneau, I. *Angew. Chem., Int. Ed.* **2007**, *46*, 8488. (c) Kim., S. H.; Yeon, J.; Halasyamani, P. S. *Chem. Mater.* **2009**, *21*, 5335. (d) Li, P. X.; Hu, C. L.; Xu, X.; Wang, R. Y.; Sun, C. F.; Mao, J. G. *Inorg. Chem.* **2010**, *49*, 4599.

(7) (a) Ra, H. S.; Ok, K. M.; Halasyamani, P. S. *J. Am. Chem. Soc.* **2003**, *125*, 7764. (b) Chi, E. O.; Ok, K. M.; Porter, Y.; Halasyamani, P. S. *Chem. Mater.* **2006**, *18*, 2070. (c) Kim., J. H.; Baek, J.; Halasyamani, P. S. *Chem. Mater.* **2007**, *19*, 5637.

(8) (a) Kong, F.; Huang, S. P.; Sun, Z. M.; Mao, J. G.; Cheng, W. D. *J. Am. Chem. Soc.* **2006**, *128*, 7750. (b) Jiang, H. L.; Huang, S. P.; Fan, Y.; Mao, J. G.; Cheng, W. D. *Chem.—Eur. J.* **2008**, *14*, 1972. (c) Zhou, Y.; Hu, C. L.; Hu, T.; Kong, F.; Mao, J. G. *Dalton Trans.* **2009**, 5747. (d) Mao, J. G.; Jiang, H. L.; Kong, F. *Inorg. Chem.* **2008**, *47*, 8498. (e) Hu, T.; Qin, L.; Kong, F.; Zhou, Y.; Mao, J. G. *Inorg. Chem.* **2009**, *48*, 2193.

(9) Phanon, D.; Gautier-Luneau, I. *J. Mater. Chem.* **2007**, *17*, 1123.

(10) (a) Sykora, R. E.; Ok, K. M.; Halasyamani, P. S.; Albrecht-Schmitt, T. E. *J. Am. Chem. Soc.* **2002**, *124*, 1951. (b) Sykora, R. E.; Ok, K. M.; Halasyamani, P. S.; Wells, D. M.; Albrecht-Schmitt, T. E. *Chem. Mater.* **2002**, *14*, 2741. (c) Shehee, T. C.; Sykora, R. E.; Ok, K. M.; Halasyamani, P. S.; Albrecht-Schmitt, T. E. *Inorg. Chem.* **2003**, *42*, 457.

(11) (a) Chang, H. Y.; Kim, S. H.; Halasyamani, P. S.; Ok, K. M. *J. Am. Chem. Soc.* **2009**, *131*, 2426. (b) Chang, H. Y.; Kim, S. H.; Ok, K. M.; Halasyamani, P. S. *J. Am. Chem. Soc.* **2009**, *131*, 6865.

(12) (a) Sun, C. F.; Hu, C. L.; Xu, X.; Ling, J. B.; Hu, T.; Kong, F.; Long, X. F.; Mao, J. G. *J. Am. Chem. Soc.* **2009**, *131*, 9486. (b) Yang, B. P.; Hu, C. L.; Xu, X.; Sun, C. F.; Zhang, J. H.; Mao, J. G. *Chem. Mater.* **2010**, *22*, 1545.

(13) (a) Meschede, W.; Mattes, R. *Z. Anorg. Allg. Chem.* **1976**, *420*, 25. (b) Ok, K. M.; Halasyamani, P. S. *Inorg. Chem.* **2005**, *44*, 2263. (c) Chen, X. A.; Zhang, L.; Chang, X. A.; Zang, H. G.; Xiao, W. Q. *Acta Crystallogr.* **2006**, *C62*, i76. (d) Sun, C. F.; Hu, C. L.; Kong, F.; Yang, B. P.; Mao, J. G. *Dalton Trans.* **2010**, *39*, 1473. (e) Sun, C. F.; Hu, T.; Xu, X.; Mao, J. G. *Dalton Trans.* **2010**, *39*, 7960.

(14) Wendlandt, W. M.; Hecht, H. G. *Reflectance Spectroscopy*; Interscience: New York, 1966.

(15) Kurtz, S. W.; Perry, T. T. *J. Appl. Phys.* **1968**, *39*, 3798.

(16) *CrystalClear*, version 1.3.5; Rigaku Corp.: Woodlands, TX, 1999.

(17) (a) Sheldrick, G. M. *SHELXTL, Crystallographic Software Package*, SHELXTL, Version 5.1, Bruker-AXS, Madison, WI, 1998. (b) Spek, A. L. *PLATON*; Utrecht University: Utrecht, The Netherlands, 2001.

(18) (a) Segall, M. D.; Lindan, P. J. D.; Probert, M. J.; Pickard, C. J.; Hasnip, P. J.; Clark, S. J.; Payne, M. C. *J. Phys.: Condens. Matt.* **2002**, *14*, 2717. (b) Milman, V.; Winkler, B.; White, J. A.; Pickard, C. J.; Payne, M. C.; Akhmatskaya, E. V.; Nobes, R. H. *Int. J. Quantum Chem.* **2000**, *77*, 895.

(19) Perdew, J. P.; Burke, K.; Ernzerhof, M. *Phys. Rev. Lett.* **1996**, *77*, 3865.

(20) Lin, J. S.; Qteish, A.; Payne, M. C.; Heine, V. *Phys. Rev. B* **1993**, *47*, 4174.

(21) Bassani, F.; Parravicini, G. P. *Electronic States and Optical Transitions In Solids*; Pergamon Press Ltd.: Oxford, 1975; 149.

(22) (a) Ghahramani, E.; Moss, D. J.; Sipe, J. E. *Phys. Rev. B* **1991**, *43*, 8990. (b) Ghahramani, E.; Moss, D. J.; Sipe, J. E. *Phys. Rev. Lett.* **1990**, *64*, 2815.

(23) (a) Duan, C. G.; Li, J.; Gu, Z. Q.; Wang, D. S. *Phys. Rev. B* **1999**, *60*, 9435. (b) Guo, G. Y.; Chu, K. C.; Wang, D. S.; Duan, C. G. *Phys. Rev. B* **2004**, *69*, 205416. (c) Guo, G. Y.; Lin, J. C. *Phys. Rev. B* **2005**, *72*, 075416. (d) Guo, G. Y.; Lin, J. C. *Phys. Rev. B* **2008**, *77*, 049901.

(24) (a) Brown, I. D.; Altermatt, D. *Acta Crystallogr.* **1985**, *B41*, 244. (b) Brese, N. E.; O'Keeffe, M. *Acta Crystallogr.* **1991**, *B47*, 192.

(25) Sun, C. F.; Hu, C. L.; Xu, X.; Mao, J. G. *Inorg. Chem.* **2010**, *49*, 9581.

(26) Nyquist, R. A.; Kagel, R. O. *Infrared Spectra of Inorganic Compounds*; Academic Press: New York and London, 1971.

(27) (a) Maggard, P. A.; Nault, T. S.; Stern, C. L.; Poeppelmeier, K. R. *J. Solid State Chem.* **2003**, *175*, 27. (b) Izumi, H. K.; Kirsch, J. E.; Stren, C. L.; Poeppelmeier, K. R. *Inorg. Chem.* **2005**, *44*, 884. (c) Sivakumar, T.; Chang, H. Y.; Baek, J.; Halasyamani, P. S. *Chem. Mater.* **2007**, *19*, 4710. (d) Chang, H. Y.; Kim, S. H.; Ok, K. M.; Halasyamani, P. S. *Chem. Mater.* **2009**, *21*, 1654.

(28) Galy, J.; Meunier, G. *J. Solid State Chem.* **1975**, *13*, 142.

(29) (a) Godby, R. W.; Schluther, M.; Sham, L. *J. Phys. Rev. B* **1987**, *36*, 6497. (b) Okoye, C. M. I. *J. Phys.: Condens. Matter* **2003**, *15*, 5945. (c) Terki, R.; Bertrand, G.; Aourag, H. *Microelectron. Eng.* **2005**, *81*, 514.